Custom Power Active Transformer for Flexible Operation of Power Systems

M.A.Elsaharty, *Member, IEEE*, Jose Ignacio Candela, *Member, IEEE*, and Pedro Rodriguez, *Fellow, IEEE*

***Abstract*—This paper presents a new transformer, i.e., the Custom Power Active Transformer (CPAT) which integrates both series and shunt power conditioning through power electronics in a single transformer. This is achieved through a distinct design of the magnetic circuit and auxiliary windings of the transformer. In this paper, a single-phase CPAT is proposed as well as a preface into its extension to multi-phase systems. Through its magnetic equivalent circuit model, several design considerations and control limitations are revealed in the paper. Analysis of the resulting CPAT structure shows some prospects in material saving as well as size and cost reduction when compared to the traditional multi-transformer based configuration. In this paper, the proposed single-phase CPAT is utilized in a distribution system application, where the control architecture is designed to attenuate voltage and current distortions at both the load and the grid side, respectively. Performance and effectiveness of the proposed CPAT are evaluated through simulation and experiments.**

***Index Terms*— Power Transformers, Magnetic circuits, Power Conditioning, Power distribution**

I. Introduction

The growing demand of electricity by customers and the high proliferation of non-linear loads exhibits serious power quality and continuity of supply issues in the power system [1]. Installation of Flexible AC Transmission Systems (FACTS) and Custom Power Devices (CPD) based on power electronics provides suitable power conditioning and compensation services to mitigate such issues in the power system. These services give rise to increased transmission capability, enhanced voltage stability and improved power quality [2], [3]. Therefore, due to the importance of such compensation devices in modern power systems, it is not only necessary to evaluate their performance, but also their efficiency, reliability, size and cost [4].

The Unified Power Flow Controller (UPFC) and Unified Power Quality Controller (UPQC) provide series and shunt compensation services to the transmission and distribution system. Such power compensation devices can be linked to the power system by using series and/or shunt transformers, which provide the flexibility of using off-the-shelf Voltage Source Converters (VSC), and satisfy required isolation requirements and winding connection options [5]–[8]. However, the increased system cost and volume of such transformers entails a trade-off to more complex non-isolated connection approaches. All these drawbacks can be solved by using integrated magnetic circuits.

Integrated magnetics have been reported in literature as coupled inductors, integrated inductor, and integrated transformers (several transformers sharing a common core) [9]. Considering FACTS and CPD applications, integrated transformers have a reduced number of magnetic components, which in turn reduces the whole system volume. Moreover, combination of several transformers into one would facilitate sub-transmission and distribution transformers with special functions, which would improve power system stability and quality.

The concept of integrating power converters into transformers was originally introduced in [10]. Recently, this concept has been further developed and improved under the name of "Smart Transformer" [11]–[12]. In this interesting approach, the use of multi-stage high-power converters does increase the controllability of the resulting system. However, the system cost increases as the power processing requirements are more demanding. Several approaches have been presented in literature to integrate power processing functionalities into transformer, which allow series voltage compensation [13]–[15], shunt reactive power compensation [16], series harmonic passive filtering [17], series power flow [18], transformer core sharing by multi-shunt power converters [19], power converter filter inductance integration [20], controllable reactor transformer [21] and series fractional power converter integration[22].

A device incorporating both series and shunt control in a single magnetic element is presented in the "Sen" transformer (ST) [23]. The ST was designed to operate as a UPFC, except for providing independent reactive power injection. The ST

consists of series-connected tap-changing windings between each phase and an exciter winding on a typical three phase core type transformer. By switching transformer taps through thyristors, addition and subtraction of induced series voltage is regulated, as well as voltage at the point of connection of the exciter winding. However, the use of taps results in a quite coarse control characteristic, and it is typically used in transmission applications.

Despite of the aforementioned developments, a method for integrating both series and shunt compensation windings into a transformer magnetic circuit, for generalized FACTS and CPD applications, has not been yet neither discussed in the literature nor published in the current state of art.

This paper presents a new active transformer concept, i.e., the Custom Power Active Transformer (CPAT), which results from equipping a passive transformer with additional auxiliary windings by following a non-conventional design of its magnetic circuit. In this paper, currents and voltages in such extra windings are actively controlled by using power converters, although they might be also drawn by using some other active or passive technique. By regulating currents and voltages in such auxiliary windings, it is possible to regulate magnetic fluxes and magneto-motive forces (mmf) in the transformer core, which in turn allows controlling current and voltage in its primary and secondary winding, respectively. These controllability degree enables the CPAT to provide advanced support services to the electrical grid through a compact transformer, being thus framed in the field of FACTS and CPD devices.

This paper is organized as follows: Section II introduces a basic configuration of a CPAT, presenting its magnetic circuit based model and analyzing its operation principle. Section III presents a CPAT working as a UPQC (CPAT-UPQC). Section IV presents a simulation-based evaluation of the CPAT-UPQC, Section V presents an experimental evaluation of CPAT-UPQC performance. Finally, some conclusions are drawn in Section VI.

II. Concept of Custom Power Active Transformer

A. Configuration

The structure and windings of a single-phase CPAT is presented in Fig. 1(a), where v_{prim}, v_{sec}, v_{sh} and v_{ser} represent the primary voltage, the secondary voltage, the shunt voltage and the series voltage, respectively. By making a simple analogy between the magnetic flux through a winding in a magnetic circuit (Φ) and the electric voltage across such a winding in an electric circuit, windings wound on a common core are equivalent to parallel-connected voltage sources, while windings wound over parallel shunt cores are equivalent to series-connected voltage sources. This analogy also entails that mmf in the magnetic circuit, represented by F in Fig. 1(a), are equivalent to currents in the electric circuit (i) [9]. Therefore, by assuming an ideal transformer with no leakage inductance and coupling factor $k = 1$, i.e. with $\Phi_0 = 0$ and $\Phi_{prim} + \Phi_{ser} + \Phi_{sec} = 0$, the equivalent electric circuit shown in Fig. 1(b) can be deduced from Fig. 1(a).

According to Ampere's law, the mmf in the primary limb of the magnetic circuit of Fig. 1(a), or in its equivalent electric circuit of Fig. 1(b), is equal to the mmf in any of other two limbs. This is mathematically expressed though (1) and (2), where F and N represent the mmf and the number of turns of windings, respectively. According to (2), for a given current circulating through the secondary winding (i_{sec}), the current circulating through the primary winding (i_{prim}) might be actively regulated by controlling the current flowing through the shunt winding (i_{sh}). Likewise, according to Gauss's law, the sum of magnetic flux from the three limbs of Fig. 1(a) should be equal to zero. This is mathematically expressed in (3) and (4), where v is the induced voltage across a winding and Φ is the flux through its core. Therefore, according to (4), for a given v_{prim}, v_{sec} can be actively regulated by controlling the voltage across v_{ser}. Control over the series winding voltage and the shunt winding current can be implemented through properly controlled power converters.

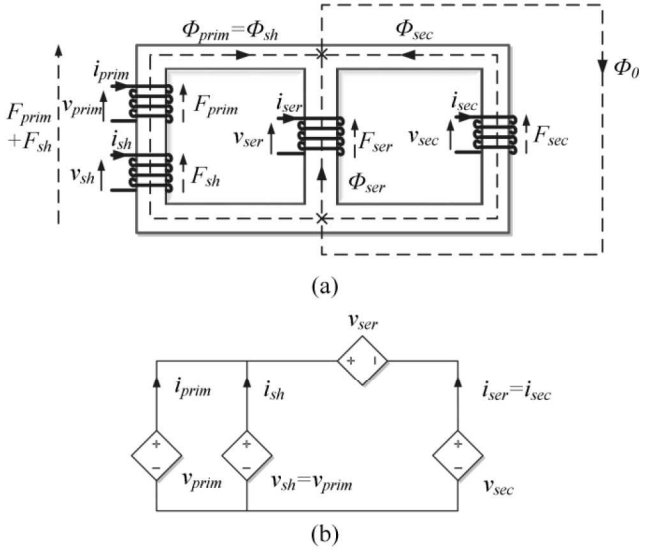

Fig. 1. Configuration of a single-phase CPAT. (a) Magnetic circuit and (b) Ideal equivalent electric circuit.

$$F_{prim} + F_{sh} = F_{ser} = F_{sec} \tag{1}$$

$$N_{prim} i_{prim} + N_{sh} i_{sh} = N_{ser} i_{ser} = N_{sec} i_{sec} \tag{2}$$

$$\Phi_{prim} + \Phi_{sec} + \Phi_{ser} = 0 \;\; ; \;\; \Phi_{prim} = \Phi_{sh} \tag{3}$$

$$\frac{v_{prim}}{N_{prim}} + \frac{v_{sec}}{N_{sec}} + \frac{v_{ser}}{N_{ser}} = 0 \;\; ; \;\; \frac{v_{prim}}{N_{prim}} = \frac{v_{sh}}{N_{sh}} \tag{4}$$

The CPAT of Fig. 1(a) could be simply extended to multi-phase systems by just interconnecting multiple single-phase transformers. However, a more effective approach in shown in Fig. 2(a), which represents a generalized layout of a multi-phase CPAT for multi-compensation purposes. In Fig. 2(a), windings are named as $tp^r{}_k$ and $np^r{}_k$, where t corresponds to the winding positive terminal dot notation, n corresponds to the winding return terminal, p indicates the phase number, r the series winding number, and k the shunt winding number. As can be observed in Fig. 2(a), each phase consists of several shunt-connected limbs, which act as several series-connected voltage

sources in the equivalent electric-magnetic circuit of Fig.2(b), while L_0 is the equivalent zero sequence return path. In such a configuration, multiple CPAT can be stacked on top of each other, each having multiple series limbs and multiple shunt windings per limb. This generalized structure reveals the possibility of having multiple shunt compensators at the primary winding, enabling a multi-converter system, which allows, for example, power exchange between different compensation windings and using low-power independent converters for each compensation objective. Moreover, series windings might have multiple shunt windings with power exchange capacity. This power conditioning configuration, with multi-shunt multi-series windings through a single core, is very flexible, since allows connecting multiple distributed power converters to a common multi-port transformer, being each converter either shunt- or series-connected to condition power between the transformer ports. Even though a detailed analysis of such multi-phase structure and its control is outside the scope of this paper, it can be used for briefly introducing a three-phase configuration for industrial applications. Three single-phase CPAT, as the one shown in Fig.1(a), can be stacked on top of each other such that each phase shares a common core yoke with another phase core. The resulting three-phase structure is similar to a three-phase shell type transformer with windings on all its core limbs, where each phase would be formed by a primary and a shunt winding wound on the its limb, a series winding wound on its central limb and a secondary winding wound on its limb. Due to the existing magnetic asymmetry between the middle phase and the other two ones in shell core structures, magnetizing currents in the three phases are unbalanced. However, the inductance of the unshared yokes is significantly large, so such current unbalance is very small. Moreover, an appropriate control of shunt and series windings allow mitigating such unbalanced to inject balanced currents into the grid.

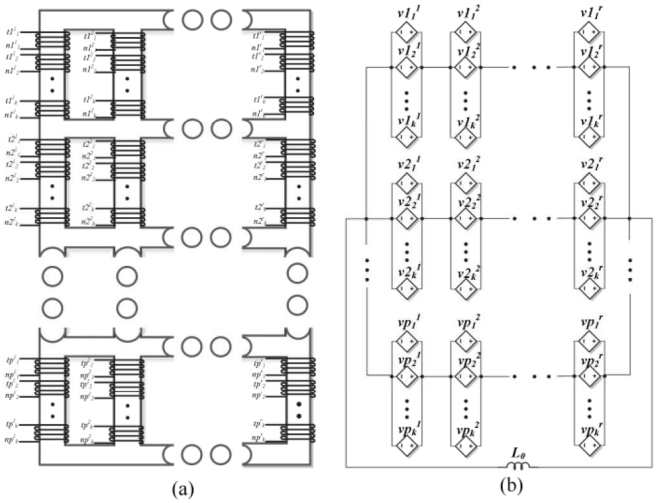

Fig. 2. Generalized layout of multi-phase multi-series/shunt auxiliary winding transformer. (a) Magnetic and winding layout and (b) Equivalent electric circuit.

B. Modelling

To model the magnetic circuit of the single-phase CPAT shown in Fig. 1 (a), a conventional approach based on using electric circuit analogy [24] will be used. The accuracy of the magnetic model depends on the assumptions made to transform the physical core into an equivalent magnetic circuit, which requires identifying magnetic paths by their corresponding reluctances. Moreover, to take into account the non-linear characteristic of the iron core, non-linear reluctances will be used to represent each core limb, while linear reluctances will be used for air paths [25].

Therefore, the magnetic behavior of a single-phase CPAT can be represented by the electric circuit shown in Fig. 3, where mmf are represented by voltage sources (F_{prim}, F_{sh}, F_{ser} and F_{sec}) and the core linkage fluxes (Φ_{prim}, Φ_{sh}, Φ_{ser} and Φ_{sec}) are represented by currents flowing in the circuit.

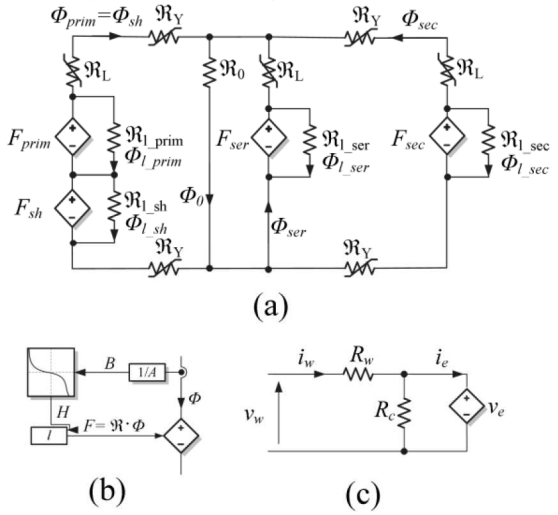

Fig. 3. Single-phase CPAT magnetic model. (a) Equivalent magnetic circuit, (b) Non-linear reluctance model and (c) Winding and core losses electrical circuit.

Leakage fluxes are categorized into core, primary, secondary, shunt and series (Φ_0, Φ_{l_prim}, Φ_{l_sec}, Φ_{l_sh}, Φ_{l_ser}) and represented by their corresponding reluctances. Linear leakage reluctance per winding ($\Re_l$) is calculated according to (5), where l is the leakage magnetic path length, A the cross-sectional area, and μ the relative magnetic permeability [26]. The non-linear core yoke reluctances $\Re_Y$ and limb reluctances $\Re_L$ are modeled by a controlled voltage source, which even gather the hysteresis characteristics of the core material, as shown in Fig. 3(b). Each winding of the magnetic circuit of Fig. 3(a) can be represented by its corresponding electric circuit as shown in Fig. 3(c), consisting of a winding resistance (R_w) and an equivalent core-losses resistance (R_c) to represent copper and core losses, respectively. Both circuits are coupled through the winding induced voltage v_e, which depends on the winding linkage flux according to (6), and the winding mmf F_e, which depends on the winding effective current i_e according to (7), being the winding number of turns represented by N_w in both equations.

$$\Re_l = \frac{l}{\mu A} \tag{5}$$

$$v_e = N_w \frac{d\Phi_e}{dt} \tag{6}$$

$$F_e = N_w i_e \tag{7}$$

C. Analysis

The following analysis is based upon considering the CPAT being used in power quality enhancement in a distribution system application. Based on the electric circuit in Fig. 3(c), Fe can be represented by (8) and limb fluxes Φ_k are represented by (9). Both equations show that winding voltage and current affect to both flux and mmf. However, the effect depends on the design parameters for the core and windings. Considering winding voltage and current consist of *n* harmonic components as in (10) and using basic magnetic circuit analysis, the effect of windings on each other can be determined.

By using the Ampere's law, the relationship between the primary limb mmf and the secondary limb mmf is shown in (11). Assuming mmf are mainly affected by currents and fluxes are mainly affected by voltages, (11) shows that harmonics in the secondary current, primary voltage and secondary voltage will yield to harmonics in the summation of the primary and shunt currents. Therefore, the shunt winding current can be properly regulated to make the primary grid current sinusoidal independently of the harmonics in the secondary current, as well as in the primary and secondary voltages. In this regard, some considerations can be taken in the design of the magnetic circuit in order to minimize the effect of the primary and secondary voltages in (11). This includes minimizing core reluctance, as well as maximizing the equivalent core-losses resistance and winding leakage reluctance.

$$F_e = N_w \left(i_w \left(1 + \frac{R_w}{R_c} \right) - \frac{v_w}{R_c} \right) \tag{8}$$

$$\Phi_k = \frac{1}{N_w} \int (v_w - i_w R_w) dt - \frac{F_e}{\Re_w} \tag{9}$$

$$v_w, i_w = \sum_{h=1}^{h=n} I_h, V_h \sin(h\omega t + \theta_h) \tag{10}$$

$$F_{e\_prim} + F_{e\_sh} = F_{e\_sec} + \left(\Phi_{prim} - \Phi_{sec} \right) (\Re_L + 2\Re_Y) \tag{11}$$

Based on Gauss's law, (12) is derived to show the effect of central limb on the magnetic circuit. As it can be observed in this equation, the summation of the primary and secondary fluxes in the transformer is influenced by the central limb flux and mmf. Therefore, the central limb flux can be properly regulated to induce those voltage components that could cancel out the effect of primary limb flux on the secondary limb flux, thereby achieving sinusoidal voltage waveforms at the secondary side, independently of the voltage distortion at the primary side. As (12) shows, the central limb magnetic performance directly dependents on the value of the core leakage reluctance ($\Re_0$). Thus, a large core leakage reluctance would allow the central limb to provide the required compensation flux with minimal control limitations.

$$\Phi_{prim} + \Phi_{ser} + \Phi_{sec} = \Phi_0 = \frac{F_{ser} - \Phi_{ser} \Re_L}{\Re_0} \tag{12}$$

From the magnetic circuit model in Fig. 3(a), a topologically correct equivalent electric circuit model can be derived through the principle of duality [25]. The electric equivalent electric circuit of Fig. 3(a) is shown in Fig. 4, with *L* representing the equivalent inductance for each reluctance and L_e representing primary and secondary core equivalent inductances. Since each inductance is inversely proportional to its equivalent reluctance, it can be observed from the circuit topology how core inductances and core leakage inductance play an important role in the performance of the CPAT. Since core inductances are represented as shunt elements, they are required to be maximized to reduce the magnetizing current of the transformer and to increase the coupling of the series compensation winding. Likewise, core leakage inductance is represented as a series element, which is required to be minimized to reduce the voltage drop through the circuit i.e. leakage flux.

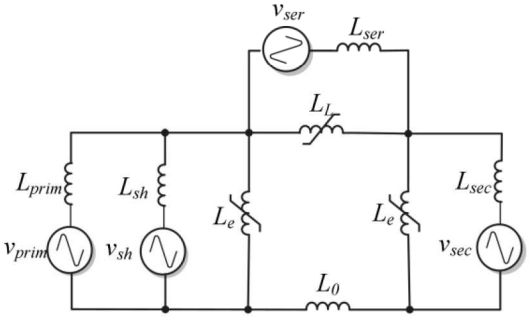

Fig. 4. Equivalent electric circuit of single-phase CPAT.

The non-linear reluctances of the core vary based upon the hysteresis loop characteristics of the core material. The non-linearity shown in Fig. 5, based on magnetic field intensity (*H*) and magnetic field density (*B*), can be classified into a saturation region and a nonlinear region. When a CPAT is utilized as a regular transformer, with shunt and series winding controllers disabled, the CPAT would operate as a typical single-phase core type transformer. Since the flux in the core due to the primary winding voltage is constant, the generated mmf will reflect the magnetizing current harmonics. In this case, the core non-linearity will draw current harmonics in the primary current due to the change in reluctance during each cycle, as shown in Fig. 6. Although the magnitude of such distorted magnetizing currents is insignificant at nominal operating conditions, a shunt winding controller can be tuned to compensate the mmf originated by them, thus canceling their effect on the primary current. Moreover, it should be noted that in case the CPAT reach the saturation region, e.g., during the transformer connections, which results in well-known inrush currents, the shunt winding mmf can be properly controlled to compensate such inrush current components, thus reducing the impact of such transient current on the grid. Thus, the effect of non-linear core reluctances can be handled by an appropriate control of the CPAT auxiliary windings.

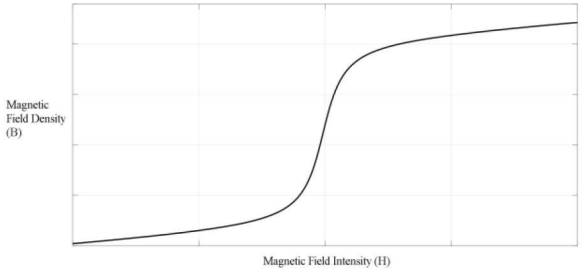

Fig. 5. Core hysteresis loop.

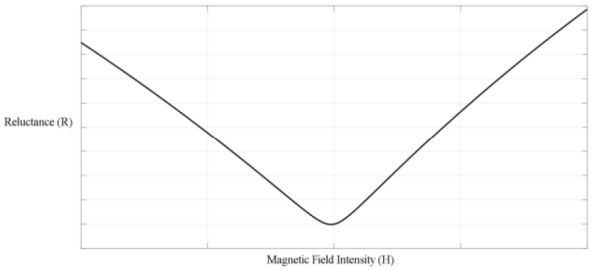

Fig. 6. Non-linear characteristics of core reluctance.

D. Assessment

The CPAT combines a shunt, a series and an isolation transformer into a single transformer. The main advantage of the CPAT over a conventional UPFC solution, based on using multiple transformers, can be summarized in terms of reduction of core material, winding and manufacturing cost.

1. Core Material Reduction

An assessment of the CPAT core material saving can be made by comparing this solution with the conventional one based on suing three independent transformers, one for voltage level transformation, one for series compensation and another one for shunt compensation. In single-phase applications, the shell type construction shown in Fig. 7 is typically utilized, consisting of one type *c* limb, two type *a* limbs and four type *b* yokes. In a conventional compensation system, three shell type transformers would be necessary. One of them would be utilized as a power transformer and the other two ones will act as compensation transformers.

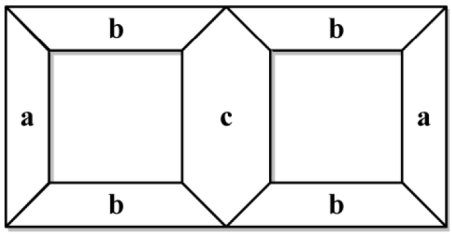

Fig. 7. Core structure of single-phase CPAT and single-phase shell type transformer.

The power transformer would have the type *c* limb larger than the other two limbs, while the compensation transformers size would depend on a core size reduction factor, which will be introduced in the following. In this assessment, it is assumed that the relationship between the core size of the power transformer (Q_p) and each compensation transformer (Q_c) is linear for all the core elements, as indicated in (13), where *m* is the core size reduction factor. Moreover, the size of the type *c* limb is assumed to be twice the size of other limbs due to its required power handling capability, while type type *a* limb and the type *b* yoke have approximately the same size. With these assumptions, the system total core size (Q_s) can be calculated as in (14).

$$Q_c = mQ_p \tag{13}$$

$$Q_s = Q_p + 2Q_c = (8 + 16m)a \tag{14}$$

A single-phase CPAT, with the configuration shown in Fig. 7, would have the same size for the *a* limb and the *b* yokes. Both of them will be larger than the *c* limb, as they handle more power. Moreover, the *c* limb is designed to have the same size of a series compensation transformer limb. Therefore, the total core size Q_T of a CPAT can be calculated as in (15).

$$Q_T = 2a + 4b + ma = (6 + m)a \tag{15}$$

Since a limb in (15) is a power handling limb, its size would be two times higher than the one obtained in (14). Taking this into account, and using the equations (14) and (15), it can be found that at m = 0.286 the CPAT would require the same material size as a conventional approach. Therefore, the CPAT would have lower costs in materials if the compensation transformers are higher than the 28.6% of the size of the power transformer.

1. Winding Reduction

Shunt and series compensation transformers in conventional applications consist of high voltage and high current windings at the grid side. However, the CPAT does not need this kind of windings, since the shunt and series compensation devices are directly coupled to the grid through the transformer core.

In a multi-transformer configuration, two windings per phase and per transformer are required. Hence, as each compensation connection requires two windings per phase, the total number of windings in a shunt-series compensation system with a power transformer would be 6*p*, where *p* is the number of phases. On the other hand, a CPAT consists of four windings per phase. Therefore, in a CPAT, the total number of windings with shunt-series compensation is 4*p*.

2. Manufacturing Cost Reduction

The combination of several transformers into a single transformer reduces the manufacturing costs related to tanks, bushings, and protection equipments, as well as the overall footprint. This is due to the fact that a solution based on several transformers would require an independent tank for each transformer, while the CPAT would eliminate the cost of compensation transformers' tank and other auxiliary equipment.

3. Comparison

The most relevant device incorporating both series and shunt control in a single magnetic element is shown in the "Sen" Transformer (ST) presented in [23]. Other approaches into magnetic integration have either discussed shunt or series integration independently. It is worth to be noted here that the CPAT can be perfectly used in transmission systems, since the shunt and series windings allow providing series power flow regulation and shunt reactive power compensation, as in a typical three-phase UPFC application.

Comparing three-phase CPAT, ST and multi-transformer configurations, the major advantages of a CPAT over the ST includes wide control bandwidth, linear response, increased number of integrated transformers, ability to provide reactive power, ability to operate for harmonics compensation and reduced number of windings.

Even though the multi-transformer approach give rise to a simpler design, CPAT and ST are better from the cost effectiveness point of view and provide a smaller and more compact solution.

III. APPLICATION OF CPAT

A. Configuration

Considering the utilization of CPAT in a single phase UPQC application (CPAT-UPQC), the configuration shown in Fig. 1 is combined with the three-phase power conversion structure presented in [8], as shown in Fig. 8. The objective of the presented UPQC is to maintain a sinusoidal voltage waveform at the load side when supplied with a distorted source voltage, as well as achieving a sinusoidal current waveform at the source side, with unity power factor, when a non-linear load connected at the secondary side.

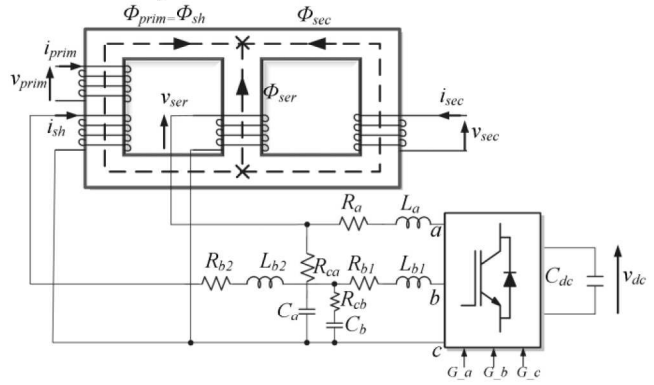

Fig. 8. Configuration of a CPAT-UPQC.

As Fig. 8 shows, the leg 'a' of the converter is connected to the series compensation winding through an LC filter, controlling the voltage across the capacitor in order to provide the required series compensation to achieve a sinusoidal voltage at the secondary side of the transformer. Leg 'b' of the converter is connected to the shunt compensation winding through an LCL filter, controlling the filter output current to provide shunt compensation and achieve sinusoidal currents at the primary side of the transformer. Leg 'c' of the converter is the current return leg for both the shunt and the series windings. This common leg for both compensation outputs presents some control challenges due to coupling between the legs. Among the strategies proposed in literature, the strategy presented in [27], based on three-leg UPQC space vector modulation (TL-UPQC SVM) is utilized due to its simplicity and effectiveness.

According to (11), if a sinusoidal grid voltage is connected to the primary winding and a non-linear load is connected to the secondary winding, the primary limb mmf (F_{e_prim}+F_{e_sh}) will consist of the same harmonics as F_{e_ser}. Moreover, further harmonics will be induced due to the non-linearity of the core reluctance. Injection of a shunt compensation current (i_{sh}) allows adjusting the required mmf from the primary winding and hence conditioning the primary current (i_{prim}) accordingly. Moreover, i_{sh} will also have a component at the fundamental frequency in order to control the DC bus voltage (v_{dc}) and compensate reactive power required from the primary winding. Furthermore, harmonics in the grid and load voltage will increase the harmonics level in F_{e_prim}+F_{e_sh} due to the effect of Φ_{prim} and Φ_{sec} according to (11).

According to (12), provided the core leakage flux is set to a minimum level through appropriate design considerations, the secondary flux Φ_{sec} can be properly regulated by controlling the series flux Φ_{ser}, i.e., by controlling the central limb winding voltage (v_{ser}). Therefore, considering v_{prim} consists of harmonic components, they can be cancelled out in the secondary winding voltage by injecting counteracting harmonic voltages through the central limb. Moreover, magnitude of the fundamental frequency of v_{sec} can be controlled by adding a fundamental frequency voltage component to the series winding voltage, which allows compensating voltage swells and sags.

B. Control

The control architecture of the CPAT is presented in Fig. 9 and Fig. 10, which consists of two controllers, namely, the shunt and the series compensation controllers. The control strategy for both controllers is based on [28], operating in the stationary reference frame. The reason for utilizing controllers in the stationary reference frame was to eliminate the requirement of synchronous transformations and directly feed the controllers by the feedback signals. Moreover, for harmonics compensation, resonant controllers have demonstrated to be a very effective solution [29].

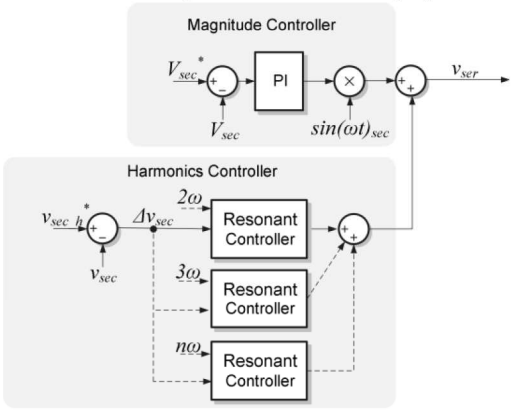

Fig. 9. Series compensation control loop of single-phase CPAT-UPQC.

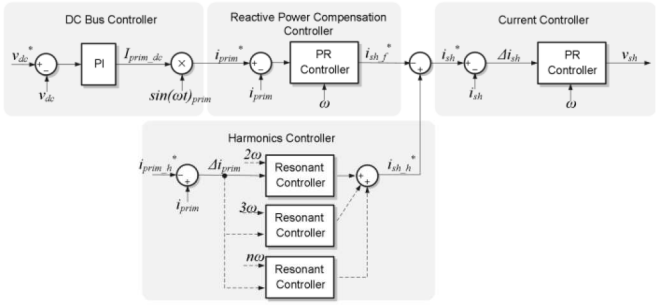

Fig. 10. Shunt compensation control loop for single-phase CPAT-UPQC.

The series compensation control loop shown in Fig. 9 consists of two parts, i.e., a magnitude controller and a harmonics controller. Magnitude of the secondary winding voltage is maintained constant through a PI controller, which is multiplied by a secondary voltage synchronizing signal ($\sin(\omega t)_{sec}$), in order to achieve an adjustable in-phase compensation of the secondary voltage magnitude. On the other hand, the secondary voltage harmonics are compensated through resonant controllers tuned at adjustable compensating frequencies, with a harmonics reference voltage $v_{sec\_h}^*$ set to zero. The resulting command voltages are added to obtain the

required voltage across the series compensation winding, which is the leg 'a' respect to leg 'c' reference voltage for the power converter.

The shunt compensation control shown in Fig. 10 consists of four controllers, i.e., two controllers for regulating the fundamental frequency component of primary current, one controller for compensating harmonic components, and one current controller for eventually regulating the current injected in the shunt winding according to the reference provided by previous controllers. The dc bus voltage controller aims to keep the bus voltage (v_{dc}^*) constant by exchanging active power with the grid through the primary side of the transformer. A PI controller set the amplitude for the required dc balancing current (I_{prim_dc}). I_{prim_dc} is synchronized with the fundamental primary voltage ($\sin(\omega t)_{prim}$) to achieve a primary reference current (i_{prim}^*). i_{prim}^* and the feedback primary current (i_{prim}) are processed by a PR controller tuned at fundamental frequency in order to obtain the required fundamental shunt compensation current ($i_{sh\_f}^*$), which guaranties constant dc bus voltage with zero-reactive power demand from the primary side and provides damping to the primary current during transients. Moreover, primary harmonic currents are compensated through resonant controllers, with a reference current $i_{prim\_h}^*$ typically set to zero. This controller set the required shunt compensation harmonic currents ($i_{sh\_h}^*$) to mitigate primary current harmonics. The combined compensation reference current (i_{sh}^*) is provided as an input to the PR controller to obtain the required shunt output voltage to by synthesized by the power converter.

In the three-phase power converter, decoupling of leg 'a' and leg 'b' voltage with respect to 'c' is achieved through the method proposed in [27] to determine the pulse width modulator (PWM) index for each leg. The primary grid frequency is obtained through a double second-order generalized integrator frequency locked loop (DSOGI-FLL) [30]. The DSOGI part is utilized with a positive/negative sequence calculation block (PNSC) to determine the synchronizing signal ($\sin(\omega t)_{prim}$), the secondary voltage magnitude (V_{sec}) and the secondary voltage synchronizing signal ($\sin(\omega t)_{sec}$), which are required for the compensation controllers discussed earlier.

IV. Simulation Results

A single-phase CPAT with parameters tabulated in Table I was simulated by using Matlab/Simulink. To examine the effectiveness of series harmonic compensation, the primary voltage was generated through a combination of harmonic components with the spectrum presented in Fig. 11.

Such severe harmonic spectrum was intentionally selected to evaluate the CPAT compensation effectiveness under extreme conditions. Shunt harmonics compensation was investigated by connecting the non-linear load shown in Fig. 12 at the terminals of the secondary winding which draws non-linear, active and reactive current with the harmonic spectrum presented in Fig. 11. Moreover, secondary voltage magnitude control was evaluated by applying voltage disruption during operation.

As shunt compensation was enabled, the non-linear current that was required by the load was compensated by the converter, in such a way that the resulting i_{prim} is sinusoidal and in phase with the primary voltage, as shown in Fig.13. In this case, the shunt converter provided the harmonic components shown in Fig. 15, which was required by i_{sec} in Fig. 14. The reactive power, which is required to magnetize the core and supply the load, was delivered through the shunt converter as shown in Table II.

The shunt controller also absorbs active power, as it can be seen in Table II, to transfer power to the series converter while maintaining a constant DC bus voltage. Moreover, it can be observed that v_{shunt} is equal to v_{prim} as in Fig. 13 and Fig. 16 since both equivalent circuits are in parallel.

The harmonic voltages in v_{prim} shown in Fig. 13 are eliminated thanks to the series controller. Hence, secondary voltage v_{sec} are free of distortions, as shown in Fig. 14.

It is worth to remark that in the simulation result it can be proven that i_{ser} is equal to i_{sec} since both are equivalent to a series circuit, as discussed in Section II. This is endorsed by the results shown in Fig. 14 and Fig. 15.

Furthermore, to demonstrate the effectiveness of the series magnitude controller, Fig. 17 shows the resulting compensation action on v_{sec} during a 25% voltage sag performed at the primary. The acquired result shows how the system keeps the voltage at the rated magnitude in v_{sec} due to the change in the fundamental component of v_{ser}, that increases in order to perform the required voltage regulation.

TABLE I
Simulation Parameters

Parameter	Value
Transformer Rated Power	50 kW
Turns Ratio	1:1
Average length of core limbs	0.45 m
Average length of yoke sections	0.2 m
Core area	0.012 m^2
System Voltage	220 V
Converter Rated Power	5 kW
Switching Frequency	10 kHz
R_a, L_a	15 mΩ, 1.5 mH
R_{ca},C_a	2 Ω, 40 µF
R_{b1},L_{b1}	60 mΩ, 6 mH
R_{b2},L_{b2}	20 mΩ, 2 mH
R_{cb},C_b	4.7 Ω, 5 µF
C_{dc}	5 µF
R_{sec},L_{sec}	1 Ω, 100mH
$R_{sec\ l}$,$L_{sec\ l}$	3 Ω, 3.5mH
R_l, $C_{sec\ l}$	5 Ω, 1.1 µF

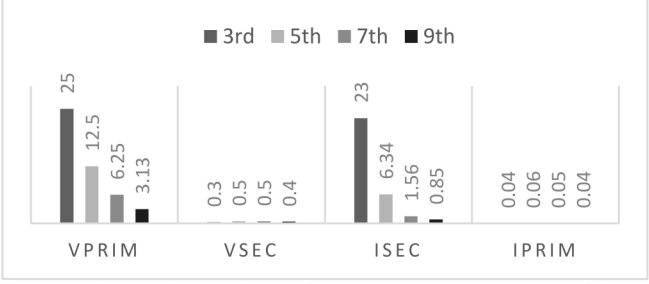

Fig. 11. Voltage and current harmonics components as a percentage of the fundamental component.

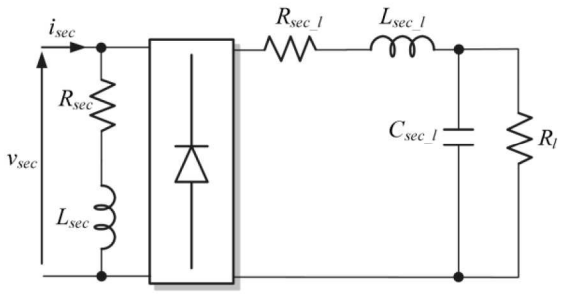

Fig. 12. Non-linear load connected at the secondary winding.

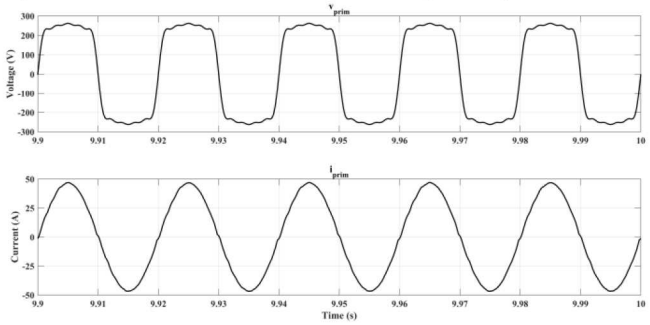

Fig. 13. Primary voltage and current waveforms.

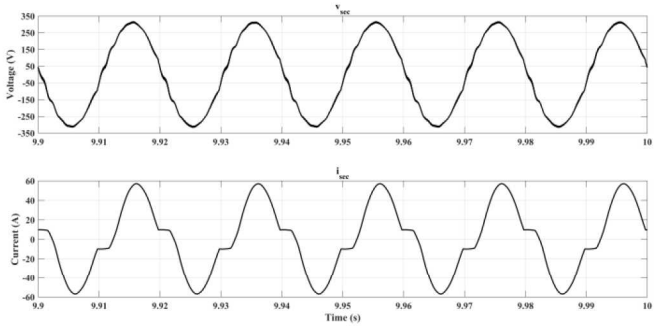

Fig. 14. Secondary voltage and current waveforms.

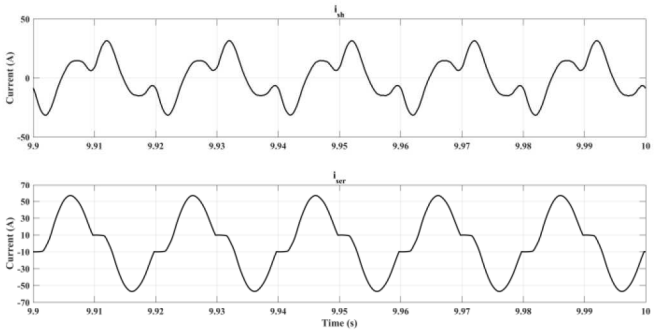

Fig. 15. Series and shunt and winding currents.

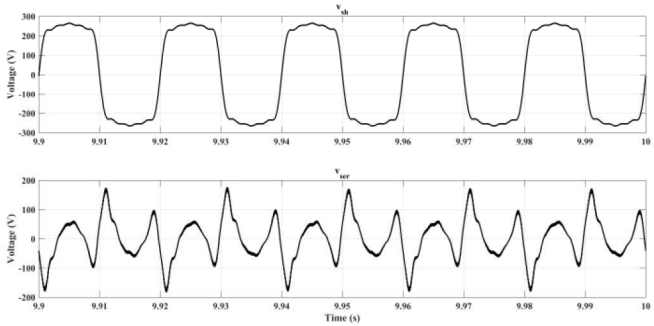

Fig. 16. Shunt and series winding voltages.

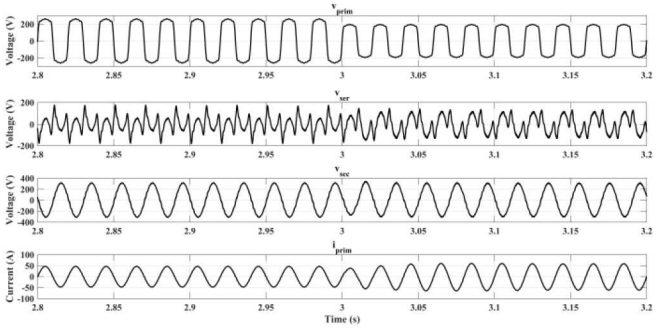

Fig. 17. Performance of the series controller under voltage sag.

TABLE II
ACTIVE & REACTIVE POWER

Winding	Active Power	Reactive Power
Primary	7.25 kW	100 VAR
Secondary	7.15 kW	2.4 kVAR
Shunt	-460 W	3.45 kVAR
Series	360 W	- 560 VAR

V. EXPERIMENTAL RESULTS

The hardware setup illustrated in Fig. 18 was implemented as shown in Fig. 19. This experimental platform consists of a 50 kW three-phase core-type transformer in which four windings were used to act as the primary, secondary, shunt compensation and series compensation of a single phase CPAT. The physical and electrical characteristics of the transformer are identical to the ones used in the simulation analysis.

In this case the primary voltage and compensating voltages are provided through a 21 kW (7 kW/phase) three-phase Power Amplifier, that emulates a power converter and its associated output filter. The three phases of the amplifier U,V,W are used such that phase U emulates the primary voltage through the reference v_{prim}^*, phase V applies a controlled v_{sh}^* based on the feedback shunt current i_{sh} and phase W applies a series compensating voltage through the reference v_{ser}^*. The control of the amplifier was performed through an OPAL Real-Time simulation platform, which includes all the control structure for shunt and series compensation. Likewise, the DC bus voltage is emulated in the real-time simulator using the amplifier phase currents iV , iW and the applied shunt, series voltage.

To investigate the effectiveness of the series compensation controller, a 100V fundamental voltage, together with a 3rd harmonic component, is applied to the primary winding, as shown in Fig.20. Moreover, this voltage is affected by a 25% voltage sag at t = 250ms.

In this study case, the magnitude controller setpoint was set to 100V, as it is indicated by the black solid lines in Fig.20. During the voltage sag, the voltage recovery is achieved as in a typical dynamic voltage regulator. This is illustrated by the fundamental series voltage injection during the sag. Moreover, the series voltage harmonic compensation manages to cancel out the effect coming from the primary harmonics, as shown in Fig.21. Therefore, the voltage harmonics elimination and magnitude regulation of the secondary voltage has been achieved experimentally as in the simulation study case, as stated in Fig. 14 and Fig. 17 respectively in the previous section.

The effect of disabling all shunt controllers with a non-linear load connected is shown in Fig.22. It can be observed how the harmonic components required by the secondary current are absorbed through the primary in normal operating conditions. As the shunt controllers were enabled, the primary current harmonics were significantly damped and the reactive power was compensated. The results available in Fig. 23 endorse clearly both statements.

Combining both experiments to operate the CPAT as a UPQC, a 3rd harmonic was injected to the reference primary voltage at 70 V. The resulting voltage and current waveforms in Fig. 24 show the ability of CPAT to effectively compensate the primary current harmonics, compensate the secondary voltage harmonics, regulate the secondary voltage as well as to maintain a unity power factor at the primary winding.

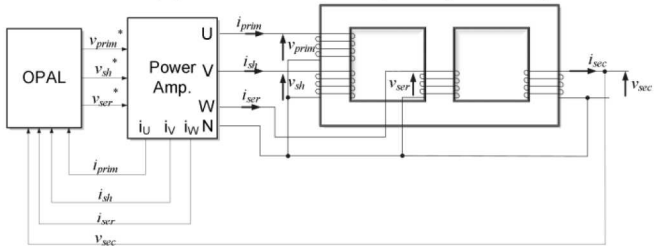

Fig. 18. Experimental setup connection.

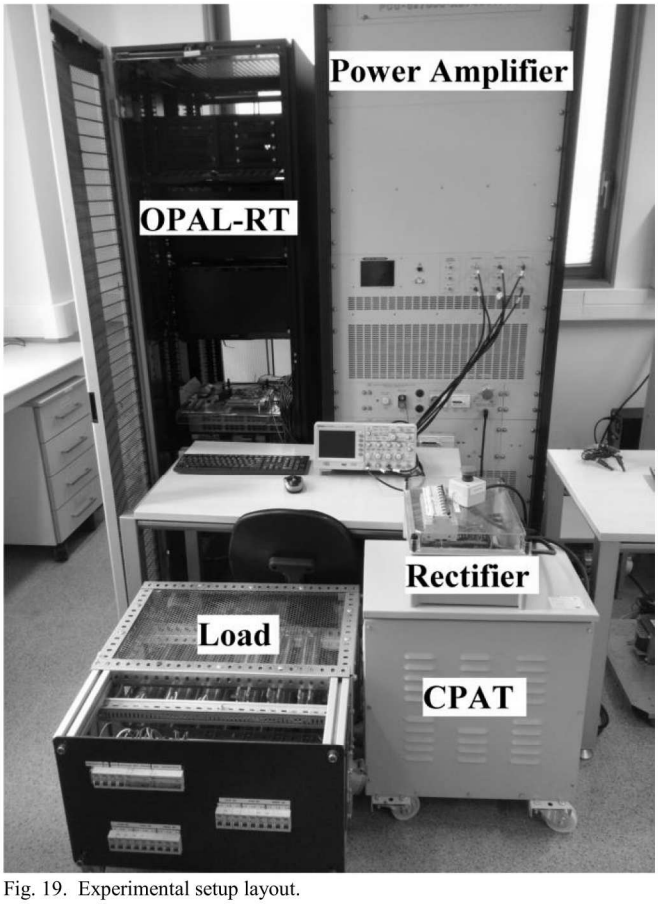

Fig. 19. Experimental setup layout.

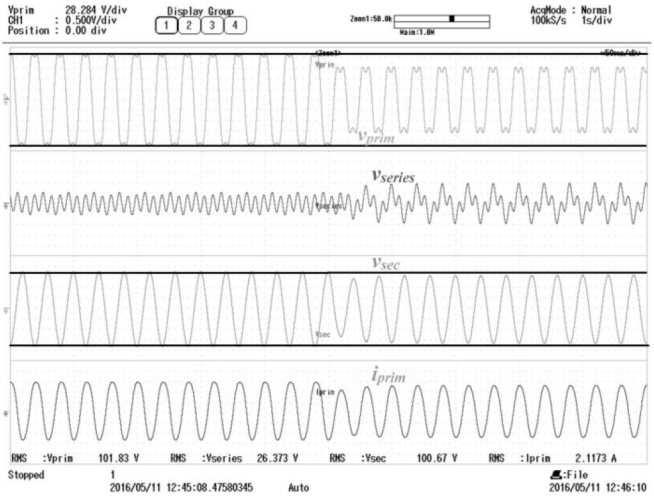

Fig. 20. Performance of series magnitude controller during a primary voltage

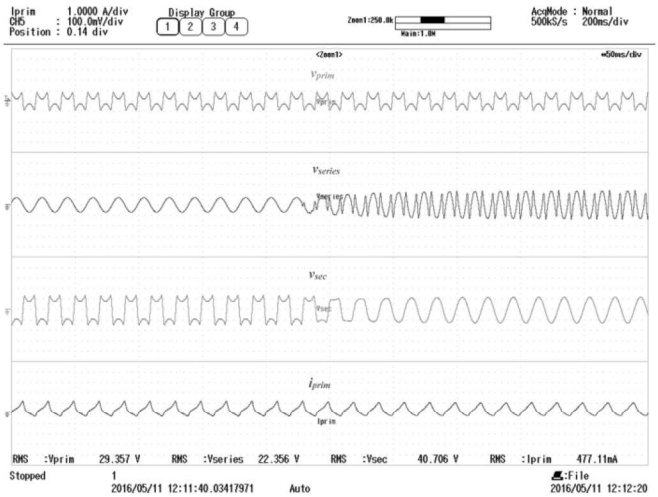

Fig. 21. Performance of series harmonic controller when enabled.

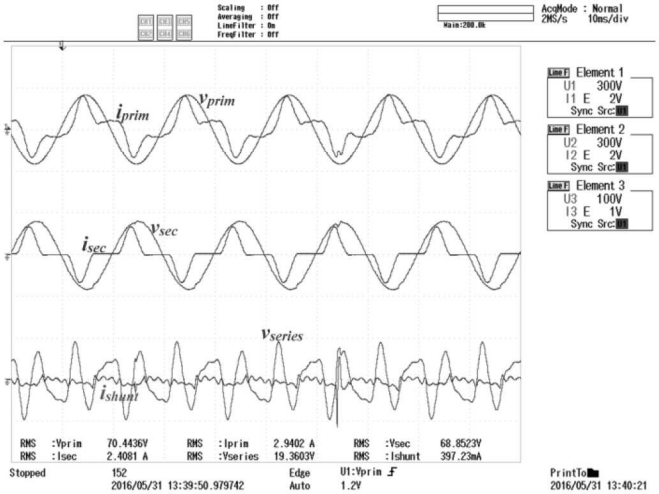

Fig. 22. Voltage and current waveforms with shunt compensation disabled. while non-linear load connected.

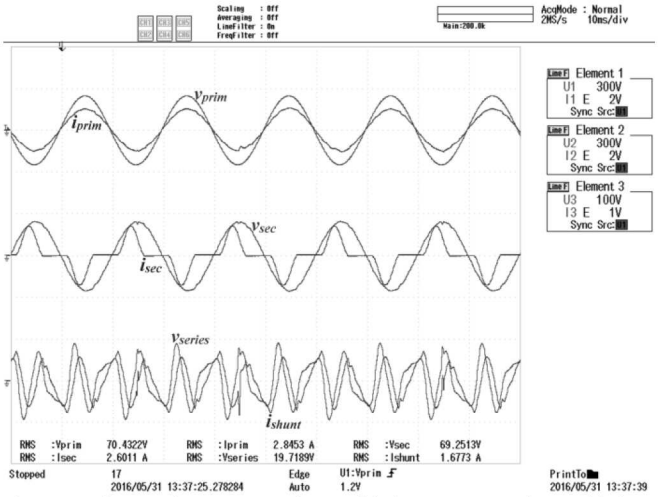

Fig. 23. Voltage and current waveforms with shunt compensation enabled while a non-linear load is connected.

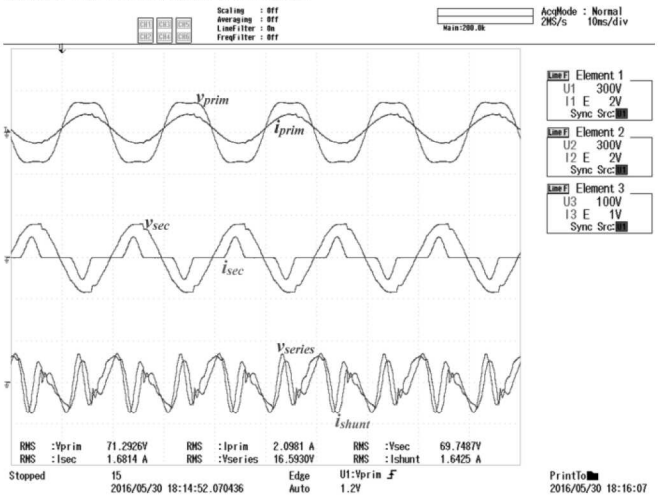

Fig. 24. Primary current and secondary voltage with both compensation controllers enabled.

VI. Conclusion

The CPAT proposed in this paper has shown the ability to combine series and shunt power conditioning in a single transformer. The effectiveness of the proposed device in terms of cost and size reduction is shown through the decrease in the equivalent core-size, number of windings and supplementary manufacturing requirements when compared to multiple transformer compensation approach. A single-phase CPAT has been presented and analyzed in terms of operation and design considerations. Moreover, the possibility for extension to three-phase and multi-phase CPAT shows the expandability of the proposed transformer. Simulation and experimental results of the CPAT-UPQC show the ability of the transformer to achieve compensation of primary current harmonics and reactive power. Moreover, the CPAT achieved secondary voltage regulation and harmonics compensation under severe operating conditions. Based on the analysis and results presented, in terms of integration of power converters in transformers, the CPAT shows a competitive and cost-effective solution.

VII. References

[1] Dennis Volk, "Electricity Networks: Infrastructure and operations," International Energy Agency, Insights Series 2013.

[2] B. R. Shperling, "Just the FACTS books on FACTS theory and insulators [review of "Introduction to the FACTS Controllers - Theory, Modeling, and Application (Sen, K. and Sen, M.L.)]," *IEEE Power Energy Mag.*, vol. 8, no. 3, pp. 96-99, May–Jun. 2010.

[3] M. L. Crow, "Power quality enhancement using custom power devices [Book Review]," *IEEE Power Energy Mag.,* vol. 2, no. 2, pp. 50-50, Mar–Apr 2004.

[4] Nasser Alemadi, Tariq Masood, R.K. Aggarwal, Suhail A. Qureshi and D.P. Kothari, "Novel Selection Approach of STATCOM Device Tailored and Optimized Engineering Configuration to Implement in Between Qatar and Bahrain," International Journal of Automation and Power Engineering, 2014, vol. 3, no. 2, pp. 75-84.

[5] B. Singh, R. Saha, A. Chandra and K. Al-Haddad, "Static synchronous compensators (STATCOM): a review," *IET Power Electronics*, vol. 2, no. 4, pp. 297–324, Jul. 2009.

[6] Y. Y. Kolhatkar and S. P. Das, "Experimental Investigation of a Single-Phase UPQC With Minimum VA Loading," *IEEE Trans. Power Del.*, vol. 22, no. 1, pp. 373–380, Jan. 2007.

[7] A. Edris, "FACTS technology development: an update," *IEEE Power Eng. Rev.*, vol. 20, no. 3, pp. 4–9, Mar. 2000.

[8] A. Nasiri and A. Emadi, "Different topologies for single-phase unified power quality conditioners," Proc. 38th IAS Annu. Meet., vol. 2, pp.976–981, Oct. 2003.

[9] Yim-Shu Lee, Leung-Pong Wong and D. K. W. Cheng, "Simulation and design of integrated magnetics for power converters," *IEEE Trans. Magn.*, vol. 39, no. 2, pp. 1008–1018, Mar. 2003.

[10] E. McMurray, "Power converter circuits having a high frequency link," U.S. Patent US3517300, Jun. 23, 1970.

[11] M. Liserre, G. Buticchi, M. Andresen, G. De Carne, L. F. Costa and Z. X. Zou, "The Smart Transformer: Impact on the Electric Grid and Technology Challenges," *IEEE Ind. Electron. Mag.*, vol. 10, no. 2, pp. 46–58, Jun. 2016.

[12] M. Liserre, M. Andresen, L. Costa and G. Buticchi, "Power Routing in Modular Smart Transformers: Active Thermal Control Through Uneven Loading of Cells," *IEEE Ind. Electron. Mag.*, vol. 10, no. 3, pp. 43–53, Sept. 2016.

[13] E. R. Ronan, S. D. Sudhoff, S. F. Glover and D. L. Galloway, "A power electronic-based distribution transformer," *IEEE Trans. Power Del.*, vol. 17, no. 2, pp. 537–543, Apr. 2002.

[14] Dayi Li, Qiaofu Chen, Zhengchun Jia and Changzheng Zhang, "A high-power active filtering system with fundamental magnetic flux compensation," *IEEE Trans. Power Del.*, vol. 21, no. 2, pp. 823–830, Apr. 2006.

[15] Wijekoon, Pinwan Thiwanka Bandara, "Power Quality Control", Patent EP20130192880, May 21, 2014.

[16] C. Wang, X. Yin, Z. Zhang and M. Wen, "A Novel Compensation Technology of Static Synchronous Compensator Integrated With Distribution Transformer," *IEEE Trans. Power Del.*, vol. 28, no. 2, pp. 1032–1039, Apr. 2013.

[17] V. Valdivia, J. Pleite, P. Zumel and C. Gonzalez, "Improving design of integrated magnetics for power electronics converters," *Electron. Lett.*, vol. 44, no. 11, pp. 693–694, May 2008.

[18] A. Dimitrovski, Z. Li and B. Ozpineci, "Magnetic Amplifier-Based Power-Flow Controller," *IEEE Trans. Power Del.*, vol. 30, no. 4, pp. 1708–1714, Aug. 2015.

[19] Robert H. Kippley, Bradley J. Schumacher, Andreas Stiedl, Kwong Kei Chin, "Multiphase Power Converters Having Shared Magnetic Core Sections," U.S. Patent US20130083575, Apr.4, 2013.

[20] G. Gohil, L. Bede, R. Teodorescu, T. Kerekes and F. Blaabjerg, "Optimized Integrated Harmonic Filter Inductor for Dual-Converter-Fed Open-End Transformer Topology," *IEEE Trans. Power Electron.*, vol. 32, no. 3, pp. 1818–1831, Mar. 2017.

[21] M. Tian, J. Yin and Y. Liu, "Magnetic Integration Technology in Controllable Reactor of Transformer Type Constituted by Various Magnetic Materials," *IEEE Trans. Appl. Supercond.*, vol. 24, no. 5, pp. 1–5, Oct. 2014.

[22] D. Das, R. P. Kandula, J. A. Muñoz, D. Divan, R. G. Harley and J. E. Schatz, "An Integrated Controllable Network Transformer—Hybrid Active Filter System," *IEEE Trans. Ind. Appl.*, vol. 51, no. 2, pp. 1692–1701, Mar.–Apr. 2015.

[23] J. Liu and V. Dinavahi, "Nonlinear Magnetic Equivalent Circuit-Based Real-Time Sen Transformer Electromagnetic Transient Model on FPGA for HIL Emulation," *IEEE Trans. Power Del.*, vol. 31, no. 6, pp. 2483–2493, Dec. 2016
[24] P.C. Sen, "Principles of Electric Machines and Power Electronics, 2nd Edition," John Wiley & Sons, 1997.
[25] S. Jazebi et al., "Duality Derived Transformer Models for Low-Frequency Electromagnetic Transients—Part I: Topological Models," *IEEE Trans. Power Del.*, vol. 31, no. 5, pp. 2410–2419, Oct. 2016.
[26] H. Dirik, C. Gezegin and M. Özdemir, "A Novel Parameter Identification Method for Single-Phase Transformers by Using Real-Time Data," *IEEE Trans. Power Del.*, vol. 29, no. 3, pp. 1074–1082, Jun. 2014.
[27] Y. Lu, G. Xiao, X. Wang, F. Blaabjerg and D. Lu, "Control Strategy for Single-Phase Transformerless Three-Leg Unified Power Quality Conditioner Based on Space Vector Modulation," *IEEE Trans. Power Electron.*, vol. 31, no. 4, pp. 2840-2849, Apr. 2016.
[28] Q. N. Trinh and H. H. Lee, "Improvement of unified power quality conditioner performance with enhanced resonant control strategy," *IET Generation, Transmission & Distribution*, vol. 8, no. 12, pp. 2114-2123, Dec. 2014.
[29] V. T. Phan and H. H. Lee, "Control Strategy for Harmonic Elimination in Stand-Alone DFIG Applications With Nonlinear Loads," *IEEE Trans. Power Electron.*, vol. 26, no. 9, pp. 2662-2675, Sept. 2011.
[30] Remus Teodorescu, Marco Liserre, Pedro Rodríguez "Grid Converters for Photovoltaic and Wind Power Systems",Wiley, 2011.

VIII. BIOGRAPHIES

M.A.Elsaharty (S'12, M'13) received the B.Sc. and M.Sc. degrees in electrical and control engineering from Arab Academy for Science, Technology, & Maritime Transport (AASTMT), Alexandria, Egypt, in 2009 and 2012, respectively. Since 2014, he has been pursuing the Ph.D. degree in electrical engineering at Renewable Electrical Energy System Research Center, Technical University of Catalonia (UPC), Barcelona, Spain. Currently, he is a Senior Teaching Assistant with the Department of Electrical and Control Engineering, AASTMT. His research interests include renewable energy systems modeling, control, and grid interface, linear and non-linear control techniques, distributed control of energy systems, active and passive power filters, power electronics converters, and robotics applications.

Jose Ignacio Candela (S'99–M'04) received the B.S. and M.S. degrees in industrial engineering and the Ph.D. degree in electrical engineering from the Technical University of Catalunya (UPC), Barcelona, Spain, in 1987, 2000, and 2009, respectively. In 1990, he became an Assistant Professor at UPC, where he later advanced to Associate Professor in 1993. Currently, he is part of the research group on Renewable Electrical Energy Systems, Department of Electrical Engineering. He has authored or co-authored more than 30 published technical papers, and holds several patents. His current research interests include power conditioning, integration of distributed energy systems, and the control of grid-connected power converters. Dr. Candela is a member of the IEEE Power Electronics Society, the IEEE Industrial Electronics Society, and the IEEE Industry Application Society.

Pedro Rodriguez (SM'10–F'13) received the M.Sc. and Ph.D. degrees in electrical engineering from the Technical University of Catalonia (UPC), Barcelona, Spain. In 1990, he joined the UPC, where he became the Director of the Research Center on Renewable Electrical Energy Systems (SEER) and still collaborates with the UPC as a Visiting Professor. In 2005, he was a Visiting Researcher with the Center for Power Electronics Systems, Virginia Tech. In 2006 and 2007, he was a Postdoctoral Researcher in the Department of Energy Technology, Aalborg University (AAU). From 2007 to 2011, he was a co-supervisor of the Vestas Power Program at the AAU. From 2011 to 2017, he was the Director of Technology on the area of power systems in Abengoa Research, Spain. Since 2017, he has been with the Loyola University Andalucia, Seville, Spain, as a Full Professor. He has coauthored one Wiley-IEEE book, more than 80 papers in ISI technical journals, and around 250 papers in conference proceedings. He is the holder of 14 licensed patents. His research interests include distributed power systems, flexible transmission systems, and power conversion. Dr. Rodriguez is an IEEE Fellow for his contributions in the control of distributed generation, an Associate Editor of the IEEE TRANSACTION ON POWER ELECTRONICS and a member of the Sustainability and Renewable Energy Committee of the IEEE Industry Application Society and the Renewable Energy Systems Technical Committee of the Industrial Electronics Society.